NUMERICAL INVESTIGATION ON THE THERMOMECHANICAL PERFORMANCES OF NANOSATELLITE ASSEMBLIES

TUDOR GEORGE ALEXANDRU[1], FLOREA DOREL ANANIA[2], CRISTINA PUPAZA[3], COSMIN GOGU[4]

Abstract: The present paper proposes a new approach for the thermomechanical analysis of small satellites. In the first stage, the heat fluxes acting on the exterior surfaces of the assembly are evaluated with the support of the CubeSat Wizard. The orbital parameters employed ensure adequate radiation heat transfer. Afterwards, the temperature distribution of the entire structure is evaluated with the support of the LISA thermal transient environment. The most critical load case is further use for calculating stress and displacement in a static analysis. Two configurations of CardSat nanosatellites are included in the study for comparison.

Keywords: small satellite, CubeSat wizard, FEM simulation, thermal analysis, static analysis

1. INTRODUCTION

Small satellites represent a miniaturized family of Low Earth Orbit (LEO) space crafts that typically weigh less than 1.5 kilograms. Their design is inexpensive and easy to customize, resulting lower manufacturing and deployment costs. Such solutions are a popular choice for educational, research, and commercial purposes. Example of missions include: Earth observation, telecommunications and scientific

[1] *Lecturer PhD Eng., Dep. of Robots and Production Systems, UNSTPB POLITEHNICA of Bucharest, Romania, alexandru_tudor_imst@yahoo.com*
[2] *Assistant Professor, PhD Eng., Dep. of Robots and Production Systems, UNSTPB POLITEHNICA of Bucharest, Romania, dorel.anania@upb.ro*
[3] *Professor PhD Eng., Dep. of Robots and Production Systems, UNSTPB POLITEHNICA of Bucharest, Romania, cristina.pupaza@upb.ro*
[4] *PhD Student Eng., MAZAROM IMPEX SRL, Bucharest, Romania, cosmin.gogu@mazarom.ro*

research [1].

Small satellites can comprise: a power system, an on-board computer, a communication system, the payload, the structural framing, an altitude determination and control system, a thermal control system and the deployment mechanism [2]. Various unit sizes are available based on the objective of the mission. The smallest form factor is 1U, which measures 10x10x10 cm by CubeSat standards [3]. This layout is useful for simple missions or test platforms. Multiple units can be employed to defined larger packages, such as 3U or 6U.

One essential requirement in the deployment and operation of small satellites consists of evaluating the structural integrity of the assembly in its early design stage [4]. Thus, numerical simulations are carried out for evaluating the response of the structure under vibrations, shock, thermal and mechanical loading [5]. Examples include the modal analysis of the primary structure for avoiding its resonance during launching [6], random vibrations for ensuring that the structure can withstand the forces and shocks that are generated by the launch vehicle [7] or the thermal analysis for capturing the temperature gradients due to the long term exposure to solar radiation or Earth's albedo [8].

From the analysis types mentioned above, the combined effect of thermal and mechanical loading is known to have adverse structural effects on the structural elements of the nanosatellite due to the resulting thermal and mechanical stress [9].

The present paper proposes a new approach for evaluating the thermomechanical performances of nanosatellites by employing two simulation environments. At first, the CubeSat wizard version 1.2 is used for evaluating the power that is absorbed by the structural elements due to radiation heat transfer. Afterwards, a FEM simulation model is developed in LISA 8.0, including the calculated heat flow rate as input. Thermal transient analysis is completed by assuming only conductive heat transfer. The simulation results are used as input in a static analysis for evaluating the stress and displacement of the studied assembly. The most critical load case is considered. Two 1U and 3U CardSat configurations are included for comparing their thermomechanical performances.

2. MATERIALS AND METHODS

2.1. Theoretical considerations

Small satellites are deployed in the low Earth orbit (LEO), which is found at less than 2.000 kilometers above the Earth's surface. In this environment, radiation represents the primary source of heat gain for space crafts. Radiative heat transfer can be distinguished as: solar radiation, earth's albedo and earth's infrared radiation.

The radiation heat transfer from a black body surface is governed by Stefan-Boltzmann's Law [10]:

$$\dot{Q}_{\max} = \sigma A T^4 \tag{1}$$

Where σ is the Stefan-Boltzmann constant, $5.67 \cdot 10^{-8}\ W/m^2 \cdot K^4$, A is the area of the surface in m^2 and T is the temperature in K. However, equation 1 is only applicable to black body. Thus, the surface emissivity is taken into account as:

$$\dot{Q}_{emit} = \varepsilon \sigma A T^4 \tag{2}$$

Where ε represents the surface emissivity.

Sunlight is a major source of power dissipation in the LEO. Its effect can be taken into account by employing [11]:

$$F_{sun} = \frac{p_{sun}}{4\pi d_{sun}^2} \tag{3}$$

Where F_{sun} represents the power released by the sun under the form of radiation, P_{sun} represents the average power output of the sun in W and d_{sun} the distance between the exposed surface of the small satellite and the sun.

Solar albedo accounts for the heat that is exchanged from the exterior surfaces of the small satellite to the Earth. The average solar albedo is estimated as 0.35. A fraction of this energy is reflected back by the Earth under the form of infrared radiation.

The amount of power that is absorbed by the structural elements of small satellites is influenced by the orbital propagation, the Right Ascension of the Ascending Node (RAAN) and the β and θ angles [12].

Orbital propagation represents the process of evaluating the satellite's position and orientation in space over time. It accounts for the satellite's motion around the Earth, including its orbit and inclination. This information is essential for calculating the satellite's exposure to solar radiation.

The Keplerian motion perturbed by the main effects of an oblate Earth equation describes the deviations from a perfect elliptical orbit experienced by a satellite due to the Earth's non-spherical shape. This equation is used to accurately predict the satellite's position and velocity over time [13].

$$\begin{aligned}
\ddot{x} &= -\frac{-\mu x}{r^3}\left\{1+\frac{3}{2}J_2\left(\frac{r_{eq}}{r}\right)^2\left(1-5\frac{z^2}{r^2}\right)\right\} \\
\ddot{y} &= -\frac{-\mu y}{r^3}\left\{1+\frac{3}{2}J_2\left(\frac{r_{eq}}{r}\right)^2\left(1-5\frac{z^2}{r^2}\right)\right\} \\
\ddot{z} &= -\frac{-\mu z}{r^3}\left\{1+\frac{3}{2}J_2\left(\frac{r_{eq}}{r}\right)^2\left(3-5\frac{z^2}{r^2}\right)\right\}
\end{aligned} \tag{4}$$

Where: J_2 represents a dimensionless parameter that quantifies the degree of the Earth's oblateness, r_{eq} represents the Earth's radius at the equator, which is slightly

larger than its radius at the poles due to the oblateness, r the distance between the satellite and the Earth's center.

The RAAN is the angle between the vernal equinox (First Point of Aries) and the ascending node, where the satellite crosses the equator from south to north. This parameter affects the satellite's exposure to solar radiation throughout the orbit, influencing the heat flux distribution on its surface [14]:

$$n = k \cdot h = \left(-h_y, h_x, 0\right)$$
$$\Omega = \begin{cases} \arccos\dfrac{n_x}{|n|}, n_y \geq 0; \\ 2\pi - \arccos\dfrac{n_x}{|n|}, n_y < 0. \end{cases} \quad (5)$$

Where: h represents the specific relative angular momentum vector, n is a vector pointing towards the ascending node and k the unit vector which is normal to the XY reference plane.

The Beta angle represents the angle between the Sun vector and the satellite's local vertical vector. It indicates the Sun's orientation relative to the satellite's zenith and significantly impacts the direct solar radiation received by the satellite's surfaces [15]:

$$\beta = \sin^{-1}\left[\cos(\Gamma)\sin(\Omega)\sin(i) - \sin(\Gamma)\cos(\varepsilon)\cos(\Omega)\sin(i) + \sin(\Gamma)\sin(\varepsilon)\cos(i)\right] \quad (6)$$

Where: Γ represents the ecliptic true solar longitude, i the orbit of inclination and ε the obliquity of the ecliptic.

The Theta angle represents the angle between the satellite's local vertical vector and the orbital velocity vector. It indicates the direction of the satellite's motion relative to the local vertical and influences the radiation heat transfer from the satellite's surface.

Together, these parameters provide a comprehensive understanding of the satellite's thermal environment, allowing for accurate calculations of surface temperature distributions. They are essential for designing thermal control systems that maintain optimal temperatures for sensitive spacecraft components and ensure the satellite's overall functionality.

2.2. The proposed approach

Figure 1 illustrates a schematic representation of the proposed approach, comprising two layers of abstraction: the CubeSat Wizard and the FEM simulation environments.

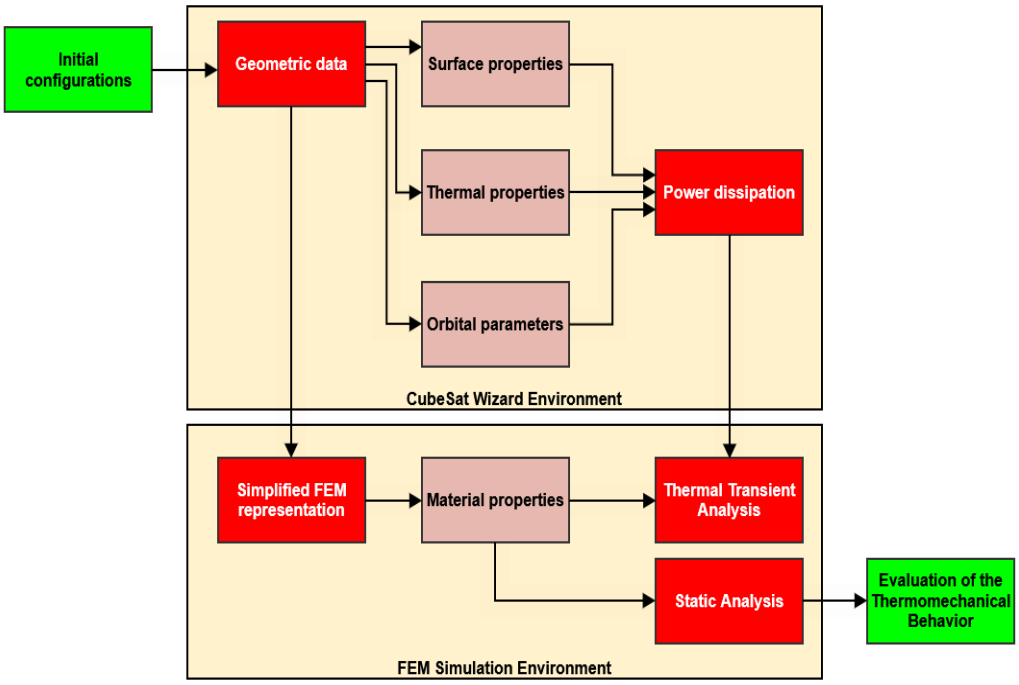

Fig.1. Schematic representation of the proposed approach

A description of the two layers is completed bellow:

2.2.1. The CubeSat Wizard environment

The initial configuration of two CardSat 1U and 3U models are used as reference. Measurement of the geometric data is carried out for defining the surface area of the solar panels and the external structural elements. Thermal characteristics are extracted from the MATWEB material database [16]. Average emissivity and absorptivity values are considered in the study by taking into account the surface coating. The outcome of the CubeSat wizard environment is to extract the total thermal loads that act on the exterior surfaces of the model.

2.2.2. The FEM Simulation environment

A simplified FEM simulation model is employed by taking into account the global dimensions of the studied assemblies. Primitive representations are used for all of the components. Two analysis types are completed: a thermal transient and a static one. In the first stage, the power dissipation resulting from the CubeSat wizard is used constraining the conductive heat transfer on the exterior surfaces of the model. The resulting temperature gradients are transferred to the static analysis by considering the worst load case scenario. Thermal stress and displacement results are retrieved for comparing the thermomechanical behavior of the studied configurations.

2.3. Overview of the studied configurations

The CARD-SAT concept has emerged from the need of developing smaller, lighter and more customizable satellites that can provide easier and more sustainable access to space. The concept follows the ongoing trend of electronic components miniaturization. CARD-SAT belongs to the pico and nano satellite family that includes a thin panel shape. With all elements included, the thickness range of this type of slim satellite starts from 1 cm [17]. CARD-SAT structures can have different sizes, from one unit (1U) to three unit size (3U) and can have different thicknesses in the range of 10 up to 40 mm (Figure 1) [18].

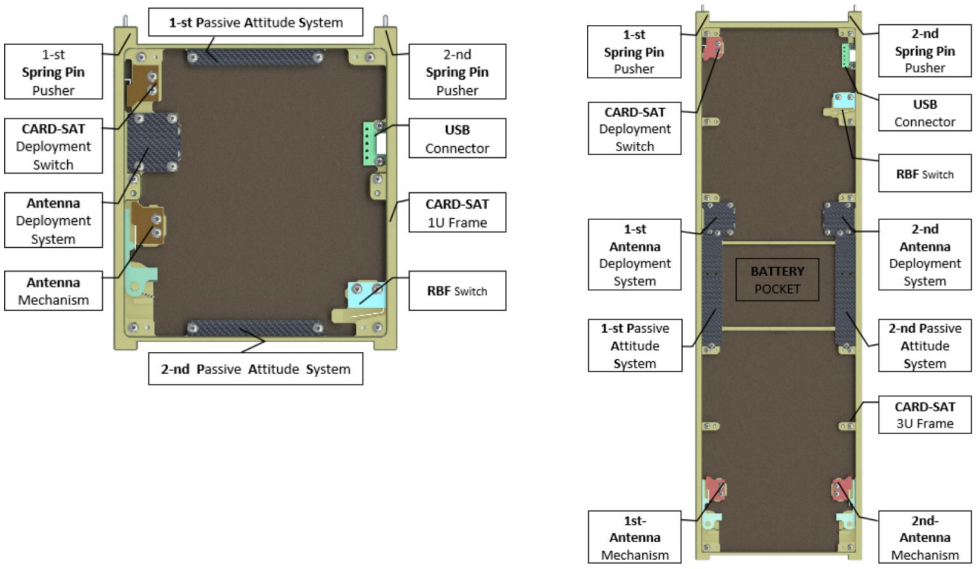

(a) (b)

Fig.1. Specifications and components of the CARD-SAT concept including – 1U (a) and 3U (b) [18]

The aluminum frame has a complex shape in order to support the payload. By standard, the micro satellite is equipped with micro switches, antennas with deployment mechanism and passive attitude system. A new deployment systems that will help launch the new CARD-SAT satellites is also available.

2.4. The CubeSat Wizard environment

CubeSat Wizard represents a freeware simulation tool that is designed to support small satellite missions emerging from various global locations [19]. The outcome of the program is to replicate orbital propagation and evaluate the thermal behavior and power generation for a certain time period, given the inputs regarding the

surface properties, thermal characteristics and orbital parameters. RAAN angle, beta angle, and altitude evolution over the time frame are simulated under orbital propagation. The tool displays the findings of thermal loading at each face and the total thermal load calculated for the entire structure. Additionally, an illustration of the temperature evolution over one orbit can be performed.

Table 1 represents the structural properties of the 1U and 3U CARD-SAT configurations.

Table 1. **Geometrical and thermal characteristics of the 1U and 3U configurations**

Parameter		**Value**	
Mass (Kg)		**1U**	**3U**
-Z / + Z Surface (Nadir and Zenith)	**Surface area (mm^2)**	862.7	862.7
	Average Absorptivity	0.8	
	Average Emissivity	0.88	
+X / -X Surface (Forward and Rearward)	**Surface area (mm^2)**	10165	33210
	Solar panel area (mm^2)	9217	30712
	Average Absorptivity	0.8	
	Average Emissivity	0.88	
+Y/-Y Surface	**Surface area (mm^2)**	1009	3055.5
	Average Absorptivity	0.8	
	Average Emissivity	0.88	

The average specific heat employed for completing the calculation is 4.56E+08 mJ/t°C.

Table 2 depicts the orbital parameters considered in the study for both configurations.

Table 2. **Orbital parameters employed in the study**

Parameter	**Value**
Inclination angle i	50
The initial value of the RAAN angle (°)	120
Initial value of the altitude h (km)	480
Rate of drop of altitude (km/day)	0.25
Type of Attitude	Nadir-pointing

The inclination angle was decided such that the satellite's orbit is closer to the equator, where the sun's rays are more direct and intense. This results in a longer period of direct sunlight exposure. On the other hand, an inclination of 50 degrees

allows the satellite to pass over a wider range of latitudes, including those near the equator where solar radiation is most concentrated. This broader coverage further enhances the satellite's exposure to solar energy. A RAAN of 124 degrees is close to the ideal value for a sun-synchronous orbit, which is an orbit in which the satellite maintains a constant angle relative to the sun. This means that the satellite will always pass over the same location on Earth at the same local time of day. Furthermore, the angle ensures that the satellite crosses the equator at the time of day when the sun is up in the sky for most locations on Earth, and therefore the satellite will receive the most direct sunlight. The initial value of altitude was chosen to fit the boundary of the LEO, at 480 km. A slow rate of drop of 0.25 km/day was decided to enhance the exposure time of the structural elements of the satellite to solar, albedo and x-ray radiation sources.

2.5. The FEM simulation environment

2.5.1 Description of the mesh

LISA FEM release 8 was employed for completing the multiphysics simulation study. In the first stage, a simplified representation strategy was employed for defining the discrete domain of the problem. Primitive bodies comprising 8-node hexahedral elements were defined for representing the frame and internal elements. On the other hand, 4 node quadrilateral elements were included to resemble the solar panel as shells. The interaction between the 2D and 3D elements is ensured by means of coincident nodes which are found in the junction area between the solar panel and the structural elements. Figure 2 a and b illustrates the resulting mesh for the two studied configurations.

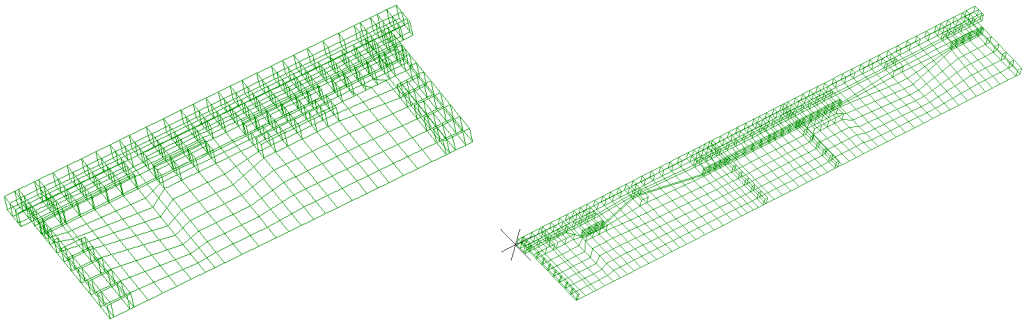

(a) (b)

Fig.2. The resulting mesh for 1U (a) and 3U (b) configurations

The computational demands of the simulation model were lowered by employing two symmetry boundary conditions. Thus, only ¼ of the model is analyzed.

2.5.2. Description of the material properties

Table 3 represents the material properties employed for completing the numerical study.

Table 3. **Material properties**

Assembly	Material	Thermal conductivity (W/mm²°C)	Specific Heat (mJ/t°C)	Modulus of Elasticity (MPa)	Poisson Ratio	Density (t/mm³)	Coefficient of thermal expansion (1/°C)
Frame	Aluminum 7075 Alloy	0.165	8.75E+08	7.1E+04	0.33	2.77E-09	2.30E-05
Antenna							
Deployment System and Altitude Control	NdFeB	0.013	1.53E+08	1.5E+04	0.24	7.01E-09	7.50E-06
Solar panel	Glass	0.0011	8.40E+08	5.1E+04	0.38	2.40E-09	6.70E-07

2.5.3. Description of the thermal transient simulation

The objective of the thermal transient analysis is to capture the temperature gradients occurring on the entire structure of the satellite. One complete orbit is considered, with a simulation time of 5544 seconds.

During this period, the variation of the θ angle will cause the heat fluxes on the exterior faces of the model to change from minimum to maximum values due to the exposure to solar, albedo and x-ray radiation. The power dissipation results from the Cubesat wizard are used for constraining the heat flow on all exterior nodes.

These boundary conditions encompass all radiation heat transfer mechanisms which occur as a single load. Thus, a temperature gradient will emerge due to the fully constrained thermal loading.

2.5.4. Description of the static simulation

The objective of the static analysis is to calculate the stress and displacement occurring due to the CTE of each defined material. In this regard, the nodal temperatures from the thermal transient analysis are imported in the static one as input loads. A free-floating boundary conditions is defined based on Figure 3.

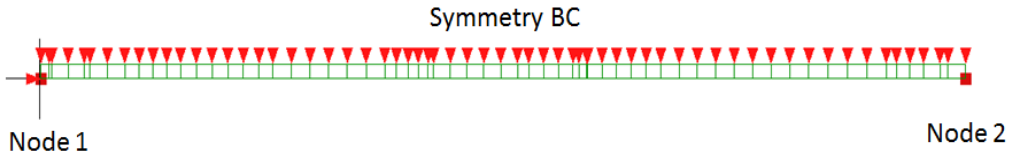

Fig.3. Description of the free floating boundary condition based on two nodes and one symmetry plane

Given the symmetry BC included, Node 1 has the TX and TY displacements constrained. In the opposite corner, Node 2 has TY displacement constrained. This technique is employed to prevent rigid body motion without restricting displacement of the assembly. Other external loads are not considered in this study.

3. RESULTS AND DISCUSSIONS

3.1. CubeSat wizard results

The maximum power dissipation occurs on the +X/-X surfaces of both configurations, due to their dominant area. Figure 4 and 5 illustrate the thermal load for a complete orbit captured at these locations for the two studied configurations.

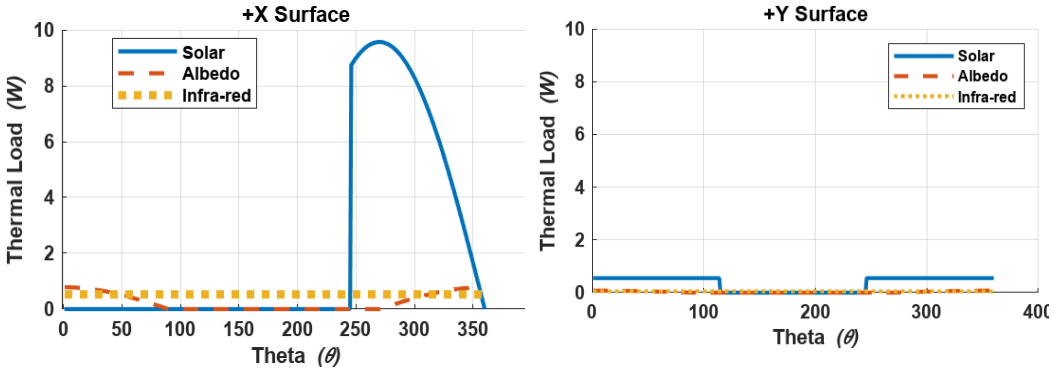

(a) (b)

Fig.4. The thermal load calculated by the CubeSat wizard for the 1U configuration for the +X (a) and +Y surfaces (b)

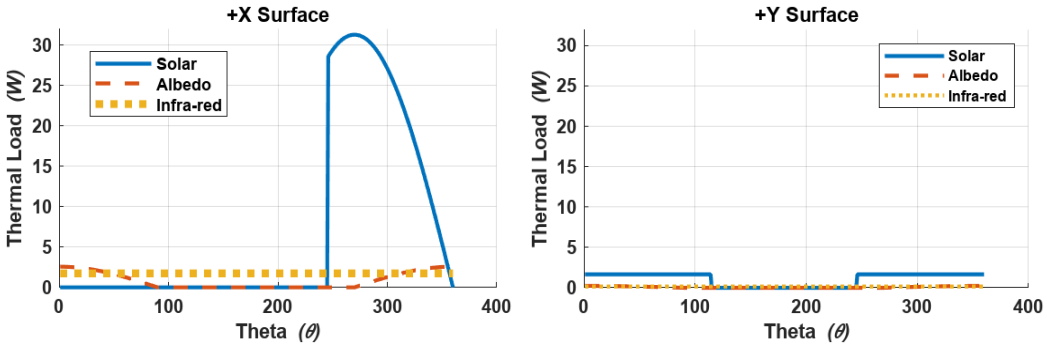

(a) (b)

Fig.5. The thermal load calculated by the CubeSat wizard for the 3U configuration for the +X (a) and +Y surfaces (b)

The average power dissipation occurring on all surfaces for a complete orbit is depicted in Table 4 for the 1U and 3U configurations.

Table 4. **Average power dissipation on all surfaces for both studied configurations**

Surface	Configuration					
	1U			3U		
	Solar (W)	Albedo (W)	Infrared (W)	Solar (W)	Albedo (W)	Infrared (W)
+/-X	7.94	0.66	1.5	16.2	1.33	1.5
+/-Y	0.66	0	0	1.33	0	0
+Z	0.03	0	0	0.08	0	0
-Z	0.22	0	0	0.66	0	0

3.2. Thermal transient results

Figure 6 depicts the temperature fringe for last time step of the transient thermal analysis for the 1U and 3U configurations.

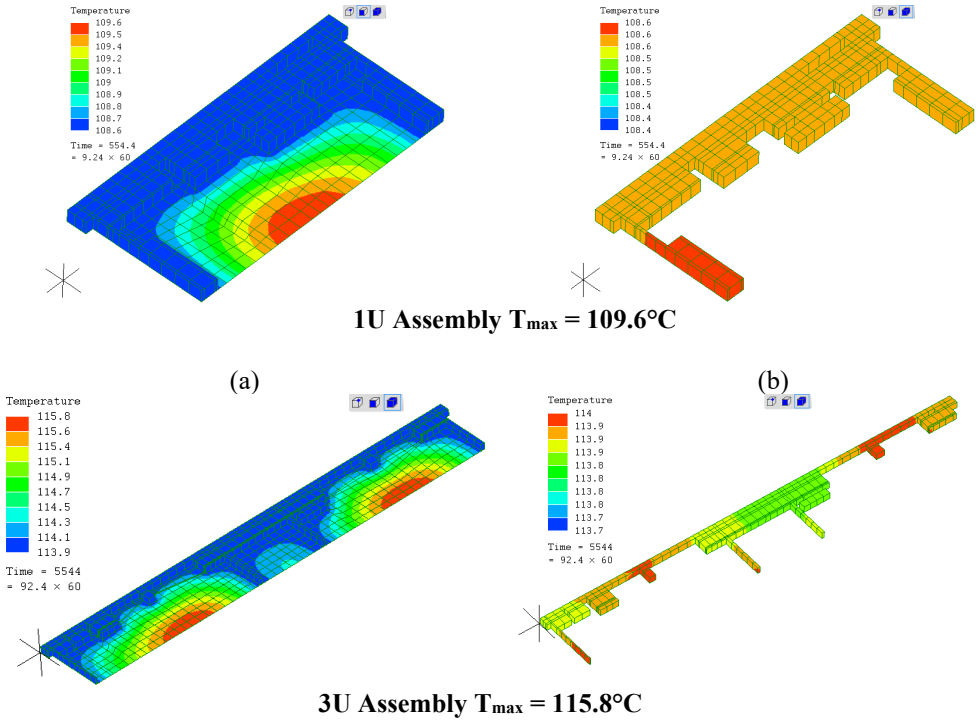

Fig.6. Temperature fringe for the 1U and 3U configuration by considering the entire assembly (a,c) and only the structural elements (b,d)

A graphical representation of the temperature curves of the two studied configurations is presented in figure 7 for the 1U and 3U configurations.

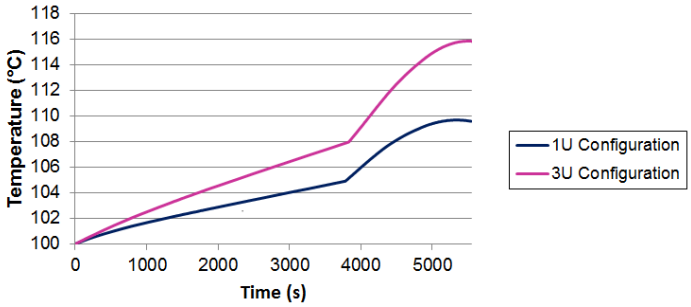

Fig.7. Comparison of the 1U and 3U temperature curves

The temperature of the 3U configuration reaches a maximum value of approximately 116°C. On the other hand, the 1U configuration is about 7°C cooler assuming the same orbital parameters. The results achieved prove that the 3U configuration has a consistently higher temperature than the 1U configuration. This suggests that the 1U configuration is more efficient in terms of heat dissipation. However, this behavior is influenced by the area of the +/-X surfaces, meaning that lower magnitude heat fluxes occur in case of the 1U configuration. A small difference can be noticed regarding the time required for the two temperature curves to reach the peak value (5159.1 seconds for the 1U instead of 5462.235 seconds for the 3U configuration).

3.3. Static analysis results

Figure 8 depicts the maximum displacement of the 1U and 3U configurations.

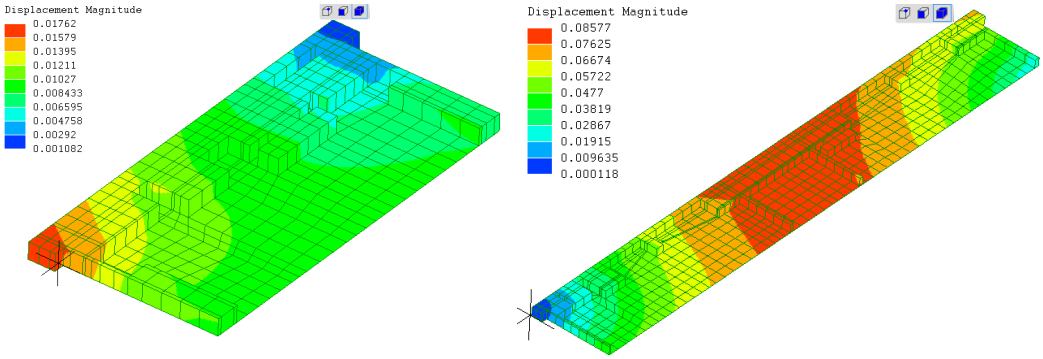

1U Configuration
Δx_{max}=0.01762 mm

(a)

3U Configuration
Δx_{max}=0.08577 mm

(b)

Fig.8. The maximum displacement of the 1U (a) and 3U configurations (b)

The maximum displacment of the 1U configuration has a value of 0.01762 mm. On the other hand, the 3U configuration achieves 0.0857 mm, which is 1.3 times greater. This behavior can be explained by the smaller surface area to volume ratio of the 1U configuration, which means that the assembly is more resistant to changes in temperature.

Figure 9 depicts the Von Mises Stress of the 1U configuration.

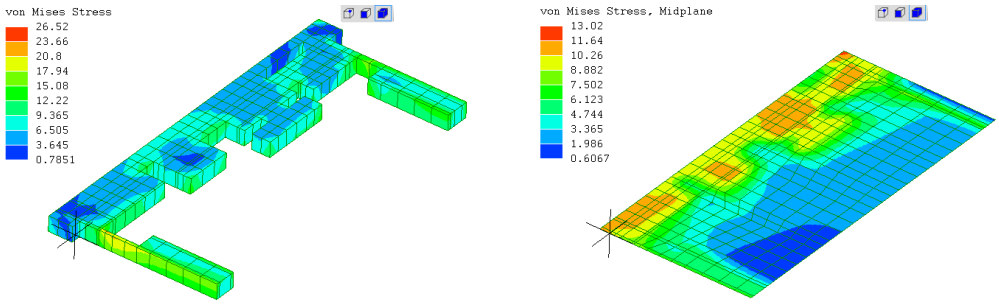

(a) (b)

Fig.9. The von Mises stress occuring due to the thermal applied loads for the 1U configuration by considering the entire assembly (a) and only the solar panel (b)

The maximum value of 26.52 MPa occurs adjacent to the –Z surface. In this location, the thickness of the wall has the minimal value. The asymetric distribution of the result can be expalined by the stiffening effect of the deployment mechanism that is found in the opposite corner. However, the stress magnitude is low compared to the tensile yield strength of Aluminum 7075 Alloy - 503 MPa. On the other hand, the maximum stress of 13.02 MPa can be noticed on the solar panel junction with the frame, adjacent to the +Z surface. Differences of 2 MPa are visibile in the stress gradient, the peak value occuring in the +Y and –Z interaction area due to the variation of the geometric shape. There is no structural integrity loss risk, given the fact that the Tensile yield strength of the solar panel glass exceeds 100 MPa.

Figure 10 depicts the Von Mises Stress of the 3U configuration.

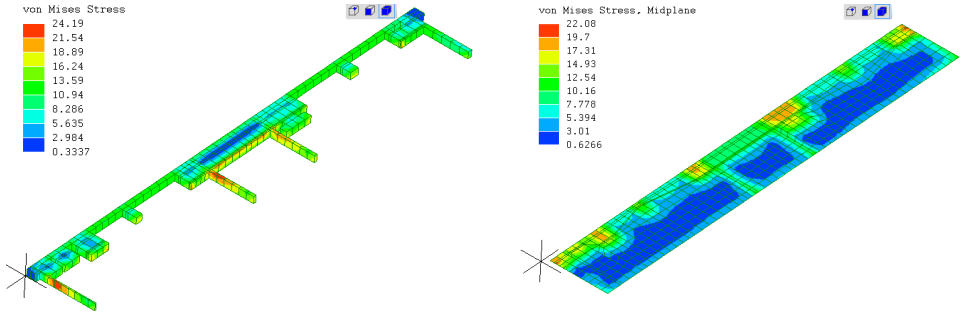

(a) (b)

Fig.10. The von Mises stress occuring due to the thermal applied loads for the 3U configuration by considering the entire assembly (a) and only the solar panel (b)

Similar to the 3U configuration, peak stress values occur in the +/-Z and +Y surface interaction areas. Even so, the location of the battery pocket and the passive altitude control system change the load distribution, resulting additional stress locations than compared to the 1U configuration. This behavior can be explained on the high differences in the CTE of the multiple materials employed in the same location. The stress magnitude on the structural elements is comparable to the one achieved in the 1U case. However, the solar panel reaches maximum values of 22 MPa. Thus, there is still no risk of structural integrity loss.

4. CONCLUSIONS

The outcome of the present paper is to conduct a comparative analysis of two nanosatellite configurations, belonging to the CARD-SAT family.

In the first stage, CubeSat wizard is employed to calculate the heat fluxes that result on the exterior surfaces of the assemblies due to the exposure to sunlight, albedo and x-ray radiation. A simplified FEM simulation model is developed by employing LISA FEM release 8.0. Hexaedral elements are used to represent the primary structure based on primitive representation. 4 node shell elements are employed for the solar panels. A rigid interaction is considered between the main components. 7075 Aluminum alloy represents the default material for the model, excluding the passive altitude system which encompasses NdFeB. Tempered glass is used for the solar panels. All material properties are extracted from the MATWEB material library.

A thermal transient analysis is completed for evaluating the temperature gradients of all assembly elements given the exterior heat fluxes as input.

In the next stage, the nodal temperatures are transferred to a static analysis. A free floating boundary condition is defined based on 2 nodes and the symmetry plane.

The results of the thermal analysis indicate that the maximum temperature of 115.8°C occurs in case of the 3U configuration. Differences of 7°C were noticed for the 1U configuration given its dimensions, and thus lower heat flux magnitudes. Both configurations reach the peak temperature in a similar amount of time.

The results of the static analysis emphasize the ability of the 1U configuration to resist to changes in temperature due to the smaller surface area to volume ratio. In terms of von Misses stress, both configurations achieve similar gradients. Even so, the location of the 3U altitude control system and the battery pocket causes load redistribution. Thus, an additional stress gradient can be observed. The Yield strength of the materials confirms that no structural integrity loss occurs. Other external loads are not taken into account.

One limitation of the methodology is the conservative assumption of 2 plane symmetry in the simulation model. As a consequence, the thermal loads are more severe than in practice.

In future work, the authors will investigate the behavior of more advanced materials (such as carbon fiber or polyetheretherketone), as an alternative to the

existing design. This will enhance the mission capabilities of the CARD-SAT family by lowering their mass, and thus deployment costs.

AKNOWLEDGMENTS

This work was supported by the 1st priority axis of "The Competitiveness Operational Program" [ID / Cod MySMIS: 120353] in the framework of "Advanced Technologies for Manufacturing and Testing of Advanced Materials in the Aerospace Domain", Contract number [402/390078/24.12.2021].

REFERENCES

[1]. **Curzi, G., Modenini, D., Tortora, P.**, Large constellations of small satellites: A survey of near future challenges and missions. *Aerospace*, *7*(9), 2020, Article: 133.
[2]. **Murugan, P., Agrawal, Y.,** Small satellites applications, classification and technologies. International Journal of Science and Research (IJSR), 9(7), 2020, pp. 1682-1687.
[3]. **Zosimovych, N.**, 1U Cubesat Platform Design. International Journal of Aerospace Sciences, *8*, pp. 1-7.
[4]. **Welle, R.P.**, The CubeSat Paradigm: An Evolutionary Approach to Satellite Design. 32nd Space Symposium, Technical Track, 2016m, pp.1-12.
[5]. **Herrera-Arroyave, J.E., Bermúdez-Reyes, B., Ferrer-Pérez, J.A., Colín, A.,** CubeSat system structural design. In 67th International Astronautical Congress. Guadalajara, Mexico, 2016, pp. 1-5.
[6]. **Barsoum, G.I., Ibrahim, H.H., Fawzy, M.A.,** Static and random vibration analyses of a university CubeSat project, Journal of Physics: Conference Series, 1264(1), 2019 Article: 012019.
[7]. **Biju, G., Sundararajan, T., Geetha, S.**, Structural Analyses for a Typical Small Satellite, In Advances in Small Satellite Technologies: Proceedings of National Conference on Small Satellite Technology and Applications, NCSSTA 2020, 2020, pp. 155-161.
[8]. **Elweteedy, A., Elmaihy, A., & Elhefnawy, A.**, Small satellite operational phase thermal analysis and design: a comparative study. INCAS Bulletin, 13(4), pp. 59-74.
[9]. **Bonnici, M., Mollicone, P., Fenech, M., & Azzopardi, M. A.,** Analytical and numerical models for thermal related design of a new pico-satellite. Applied Thermal Engineering, 159, 2019, Article 113908.
[10]. **Raslan, A., Michna, G., & Ciarcià, M.**, Thermal Simulation of a CubeSat. In 2019 IEEE International Conference on Electro Information Technology (EIT), 2019, pp. 453-459
[11]. **Khater, A.A.,** Temperature Distribution in CubeSats using the Finite Element Method (Doctoral dissertation, Master Thesis).
[12]. **Davoli, F., Kourogiorgas, C., Marchese, M., Panagopoulos, A., Patrone, F.,** Small satellites and CubeSats: Survey of structures, architectures, and protocols, International Journal of Satellite Communications and Networking, 37(4), pp. 343-359.
[13]. **Yedavalli, R. K.,** *Flight Dynamics and Control of Aero and Space Vehicles*. John Wiley & Sons.
[14]. **Hu, W.**, *Fundamental spacecraft dynamics and control*, 2015, John Wiley & Sons.

[15]. RM, S., Computation of eclipse time for low-earth orbiting small satellites. *International Journal of Aviation, Aeronautics, and Aerospace*, *6*(5), Article 15.
[16]. ***, MATWEB Material Property data, Retrieved online 1 December 2023 from https://www.matweb.com
[17]. Totu, A., Small-size artificial satellite - "card-sat", United States Patent Application Publication: US 2020/0391886 A1, 2020
[18]. MAZAROM IMPEX SRL, CARD-SAT Solution. Retrieved online November 30, 2023, from https://www.card-sat.com/index.php/en/
[19]. Jarrar F., Almazrouei A., Ansari M., CubeSat Wizzard App, Retrieved online 1 December 2023 from https://www.cubesatwizard.com